International Journal of Pharmaceutics 664 (2024) 124593

Contents lists available at ScienceDirect

International Journal of Pharmaceutics

journal homepage: www.elsevier.com/locate/ijpharm

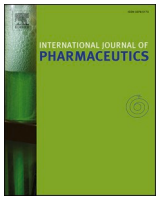

Synergistic antifungal activity against *Candida albicans* between voriconazole and cyclosporine a loaded in polymeric nanoparticles

Victoria Martín [a], Rafael R. de la Haba [b], Pilar López-Cornejo [a], Manuel López-López [c], José Antonio Lebrón [a], Eva Bernal [a], Natalia Baeza [a], Sara Ruiz [a], Francisco José Ostos [a], Vicente Merino-Bohorquez [d], Sylvie Chevalier [e], Olivier Lesouhaitier [e], Ali Tahrioui [e], Francisco José Montes [a], Teresa Sánchez-Carrasco [a], María Luisa Moyá [a,*]

[a] Department of Physical Chemistry, University of Seville, C/Profesor García González 1, Seville 41012, Spain
[b] Departament of Microbiology and Parasitology, Faculty of Pharmacy, University of Seville, C/Profesor García González 2, Seville 41012, Spain
[c] Department of Chemical Engineering, Physical Chemistry and Materials Science, Faculty of Experimental Sciences, University of Huelva, Campus de El Carmen, Avda. de las Fuerzas Armadas s/n, Huelva 21071, Spain
[d] Department of Pharmacology, University of Seville, C/Profesor García González 2, Seville 41012, Spain
[e] Univ Rouen Normandie, Université Caen Normandie, Normandie Univ, CBSA UR4312, Rouen F-76000, France

ARTICLE INFO

Keywords:
Cyclosporine A
PEG
PLGA
Polymeric nanoparticles
Synergism
Voriconazole

ABSTRACT

The goal of this work is to investigate if the synergistic antifungal activity between cyclosporine A, CsA, and voriconazole, VRZ, increases when both drugs are encapsulated in a nanocarrier as compared when they are free. The preparation and characterization of blank and VRZ and CsA loaded polymeric based PLGA nanoparticles (PLGA, PLGA-PEG, and PLGA+PEG) was a necessary previous step. Using the more suitable NPs, those of PLGA, the antifungal susceptibility tests performed with VRZ-loaded PLGA NPs, show no significant increase of the antifungal activity in comparison to that of free VRZ. However, the synergistic behavior found for the (VRZ+CsA)-loaded PLGA NPs was fourfold stronger than that observed for the two free drugs together. On the other hand, the investigation into the suppression of *C. albicans* biofilm formation showed that blank PLGA NPs inhibit the biofilm formation at high NPs concentrations. However, a minor effect or even a slight biofilm increase formation was observed at low and moderate NPs concentrations. Therefore, the enhancement of the biofilm inhibition found for the three tested treatments (CsA alone, VRZ alone, and VRZ+CsA) when comparing free and encapsulated drugs, within the therapeutic window, can be attributed to the drug encapsulation approach. Indeed, polymeric PLGA NPs loaded with CsA, VRZ, or VRZ+CsA are more effective at inhibiting the *C. albicans* biofilm growth than their free counterparts.

1. Introduction

Fungal infections are a worldwide problem being a growing threat to public health. In many cases, these infections are superficial, but some species originate life-threatening illnesses (David et al., 2022; Gushiken et al., 2021; Otto and Green, 2020; Vila et al., 2020). The distribution of the fungal infections depends on several factors, but the most common mycoses are those caused by *Cryptococcus* spp., *Candida* spp., and *Aspergillus* spp. (WHO, 2022). Those opportunistic pathogens possess the ability to form biofilms, that is, assemblages of surface-associated microbial cells enclosed into an extracellular polymeric substance matrix. Biofilm formation not only provides protection from environmental stress, but it also enhances the resistance of microorganisms to antimicrobial agents (Wu et al., 2017).

In the 1990 s several new antifungal drugs were prepared, including fluconazole and itraconazole, which changed the way of treating many fungal diseases. However, both drugs presented serious limitations and side problems (Johnson and Kauffman, 2003). With the goal of improving antifungal treatments, second-generation triazole agents were developed. Voriconazole, VRZ, is a derivative of fluconazole, where one of the triazole rings was replaced by a fluorinated pyrimidine and a methyl group was added (see Fig. 1). This resulted in an expanded activity (Johnson and Kauffman, 2003; Donnelly and de Pauw, 2004). However, with the widespread use of antifungal agents, fungal drug

* Corresponding authors.
E-mail address: moya@us.es (M. Luisa Moyá).

https://doi.org/10.1016/j.ijpharm.2024.124593
Received 22 May 2024; Received in revised form 14 August 2024; Accepted 14 August 2024
Available online 19 August 2024

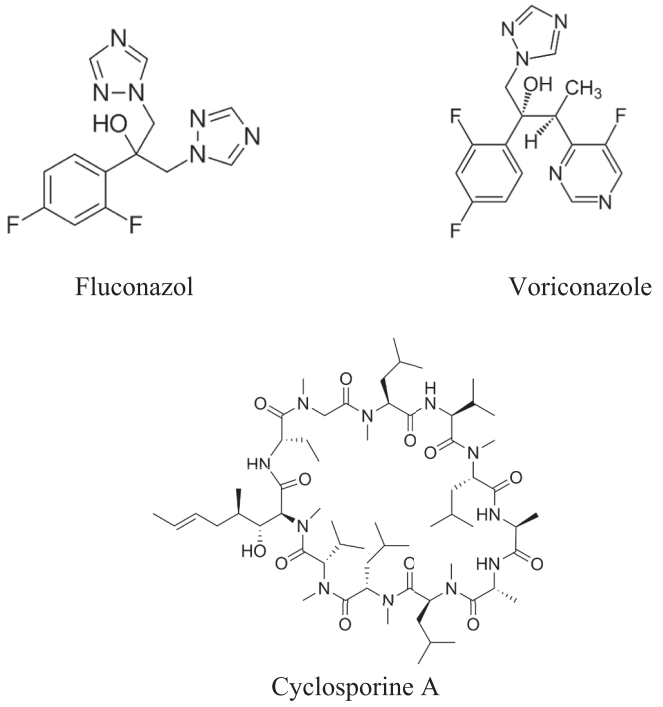

Fig. 1. Structures of fluconazole, voriconazole, and cyclosporine A.

resistance is unfortunately more and more common. Additionally, biofilm formation has been found one of the causes of fungal resistance, given that planktonic cells are over 1000 times more susceptible to common antifungal agents than matrix enclosed cells (Taff et al., 2012; Zhang et al., 2013; Akbari and Kjellerup, 2015). This, together with the adverse effects or toxicities of the available antifungal agents, particularly after long treatments (Cheng et al., 2020; Shi et al., 2019; Theuretzbacher et al., 2006), has also limited their use in clinical practice. Therefore, the overcoming of drug resistance has become a paramount issue.

Cyclosporine A (see Fig. 1), CsA, is used as immunosuppressor (Rosa et al., 2023; Deleuran et al., 2024). However, it also has other uses such as anti-inflammatory, antiviral and in dry eye disease (Guareschi et al., 2024; Locatelli et al., 2024; Uppuluri et al., 2008). Experimental studies have shown that CsA can increase the antifungal activity of various azoles, Including VRZ, being able to inhibit both planktonic and biofilms (Uppuluri et al., 2008; Shinde et al., 2012; Cordeiro et al., 2014; Nurrokhman Baly et al., 2015; Jia et al., 2016). That is, there is a synergistic behavior between antifungal agents and CsA.

Nanotechnology can provide a new approach to overcome the side effects and less favorable pharmacological properties of several antifungals. The use of nanocarriers began in 1990, with the amphotericin B preparation of lipid formulations (Voltan et al., 2016). Since then, numerous nanosystems have been prepared as nanovehicles for several antifungal drugs (de Almeida Campos et al., 2023; Kaur et al., 2021; Mohammadzadeh et al., 2021; Nami et al., 2021; Jangjou et al., 2022), these studies showing important improvements in the antifungal activity, increasing their effectivity, and reducing their toxicity, as well as in preventing biofilm formation (Taff et al., 2012; de Almeida Campos et al., 2023; Khare et al.,2016; Radwan et al., 2017). CsA has also been encapsulated in several nanosystems, which increases its aqueous solubility and improve its therapeutic effects (Badihi et al., 2020; Goyal et al., 2015; Duber et al., 2020; Li et al., 2023).

Several research articles can be found in the literature about the use of nanothechnology for the enhancement of the therapeutic effects of both VRZ and CsA as well as about the synergistic effect between these two drugs in solution, as was commented above. Nonetheless, the influence of encapsulating VRZ and CsA together in nanocarriers on the synergistic effect between the two drugs has not been investigated until now, to the authoŕs knowledge. The goal of this work is to investigate this issue. For doing so, three types of polymeric nanoparticles, NPs, PLGA (poly(lactic-*co*-glycolic acid), PLGA-PEG (polyethylene glycol) methyl ether-block-poly(lactide-*co*-glycolide)), and PLGA+PEG (PEG is polyethylene glycol) have been prepared and characterized. In this work the antifungal and anti-biofilm formation activities of free and loaded VRZ PLGA NPs, alone and in combination with free and loaded CsA PLGA NPs, respectively, were examined using a reference strain of the yeast *Candida albicans*. PLGA NPs were the more suitable NPs to carry out these studies. Our results indicate that the therapeutic activity of (VRZ+CsA)-loaded PLGA NPs increases in comparison with the synergistic effect of the free VRZ+CsA combined compounds.

2. Materials and methods

2.1. Materials and microorganisms

Poly(lactic-*co*-glycolic acid), PLGA (RG 502H), (polyethylene glycol) methyl ether-block-poly(lactide-*co*-glycolide), PLGA-PEG, polyvinyl alcohol, PVA, with an average molecular weight within the range 30,000–70,000 Da, polyethylene glycol, PEG, with an average molecular weight of 8000 Da, and VRZ were purchased from Sigma and used as received. CsA was from Acofarma. The rest of the reagents utilized in the preparation of the NPs as well as in the preparation of the buffer were also from Sigma.

All aqueous solutions were prepared with deionized MilliQ water (resistivity > 18 MΩ).

The yeast strain *Candida albicans* ATCC 10231, which is described as VRZ resistant, used for testing antifungal susceptibility and inhibition of biofilm formation, was purchased from the American Type Culture Collection (Mannasas, VA, USA). To ensure purity, cells were plated onto Yeast Extract–Peptone–Dextrose (YPD) agar, with the following composition (g/L): yeast extract (10), proteose peptone no. 3 (20), glucose (20), agar (20). The pH of the medium was adjusted to 5.6 with 1 M HCl.

2.2. Methods for preparation of nanoparticles

2.2.1. Preparation of PLGA nanoparticles

PLGA NPs were prepared by using the emulsion/evaporation method (Pinto Reis et al., 2006). PLGA at 50 mg were dissolved in 5 mL of ethyl acetate by magnetic stirring, with or without different amounts of VRZ, CsA, or both. The resulting solution was added dropwise to 20 mL of an aqueous solution containing 1.5 % (w/v) of PVA under continuous magnetic stirring at 600 rpm. The resulting emulsion was kept overnight at room temperature, under continuous stirring, in order to evaporate the organic phase, which resulted in the formation of the polymeric NPs. The remaining NPs aqueous dispersion was introduced in an Eppendorf Concentration plus, under vacuum, for 40 min to assure the total evaporation of the organic phase. Subsequently, the blank and loaded polymeric NPs were recovered by centrifugation at 13.500 rpm for 15 min. The NPs were washed twice with water to remove the non-encapsulated drugs and the volume of the supernatants was measured and, afterwards, they were kept in the fridge. The NPs obtained were dried under vacuum using the Eppendorf Concentrator plus for two–-three hours.

2.2.2. Preparation of PLGA-PEG nanoparticles

The method used was similar to that described for the PLGA NPs. The only difference is that, in order to dissolve the polymer PLGA-PEG in the ethyl acetate, 100 μL of water were added to the organic phase.

2.2.3. Preparation of PLGA+PEG nanoparticles

The method used was similar to that utilized in the preparation of the

PLGA NPs. However, in this case, the organic phase, with or without drugs, contained the PLGA, while 3.3 mg of PEG were dissolved in the 20 mL of 1.5 % of PVA. The rest of the procedure was the same as indicated above.

2.3. UV–visible spectroscopy measurements

These measurements were carried out using a Shimadzu UV-1800 spectrophotometer, connected to a water flow Lauda cryostat, with the goal of determining the amount of VRZ encapsulated within the prepared NPs. The stability of VRZ aqueous solutions was studied measuring the absorbance at $\lambda = 256$ nm, the maximum absorbance wavelength. The solutions were stable for more than one week at 298 K. A standard quartz cell of 10 mm path length was used.

A calibration curve was done in deionized water by using standard VRZ solutions within the concentration range 5–85 μg/mL. An additional calibration curve was obtained in Tris/HCl buffer at pH 7.4, Tris being tris(hydroxymethyl)aminomethane. This curve was necessary to determine the amount of VRZ in the *in vitro* drug release experiments (see below). The maximum absorbance wavelength was 256 nm.

2.4. HPLC measurements

To determine the amount of CsA encapsulated in the synthesized NPs, high performance liquid chromatography measurements were used. The HPLC-UV equipment employed was a Hitachi LaChrome Elite ®, with a LiChosper RP-18 (5 μm) C-18 reverse column. The mobile phase consisted of a 60–40 acetonitrile-(1 %phosphoric acid aqueous solution) (v/v) mixture, at a flow rate of 1.8 mL/min. CsA was detected by its UV absorbance at 214 nm. The injection volume was 20 μL and the retention time of CsA was 12.47 min. The limits of detection, LOD, and quantification, LOQ, were 0.009 and 0.30 mg/mL, respectively. All standards and samples were prepared in a mixture of similar composition than that of the mobile phase.

2.5. Size and zeta potential, ξ

A Zetasizer Nano ZS Malvern Instrument (located at the General Services of the University of Seville, CITIUS) was used to get information about the size distribution and zeta potential (ξ) of the prepared NPs. A scattering angle of 90° was utilized in the size distribution studies. The polymeric NPs were dispersed in water, at a concentration suitable to obtain reliable measurements. At least six measurements were done for three independent samples, both for zeta potential and size distribution determinations. The average value (standard deviation) was considered.

2.6. Encapsulation efficiency, %EE

The encapsulation efficiency (%EE) was calculated by using eq. (1):

$$\%\,\mathrm{EE} = \frac{mass\ \ drug\ \ encapsulated}{Total\ \ mass\ \ drug} x100 \quad (1)$$

here *mass drug encapsulated* is the amount of drug encapsulated and *Total mass drug* was the total amount of drug present in the preparation of the NPs.

In the case of VRZ, the former was calculated by subtracting the VRZ left in the supernatant when the drug loaded NPs were removed. This amount was determined by UV–visible spectroscopy at 256 nm, using the calibration curve.

CsA encapsulation efficiency was calculated by using HPLC measurements. In order to do so, a previous digestion of a known amount of loaded NPs was required. This digestion was carried out as follows: about 8 mg of dry CsA-loaded NPs were weighted in a Kjeldahl tube. Then 925 μL of ethyl acetate were added and the tube was introduced in an ultrasonic bath for 10 min. Subsequently, 10 mL of an aqueous solution of 10 % (w/v) of ethanol was added to the tube and immediately sonicated for one hour. Once the aqueous and organic phases were separated, the aqueous phase was decanted and removed. The organic phase was then introduced in an Eppendorf Concentrator Plus and totally evaporated under vacuum. The remaining CsA was then dissolved in the mobile phase and its amount determined by HPLC using a calibration curve.

It is worth noting that when VRZ and CsA are encapsulated together, the determination of the %EE for both drugs was done following the same procedures described above, since there is not interference of either of them in the methods used.

2.7. Synthesis yield, %R

The yields of the syntheses (%R) used to prepare the different unloaded and loaded NPs, were calculated by using eq. (2):

$$\%R = \frac{\text{mass NPs}}{(\text{mass of polymers} + \text{mass of drugs})} \text{ x } 100 \quad (2)$$

where mass NPs are the mg of nanoparticles obtained in each synthesis, mass of polymers and mg of drug are the initial amounts of polymer (or of polymers in the case of PLGA+PEG NPs) and drug (or drugs if VRZ and CsA are encapsulated together) used in the preparation, respectively.

2.8. Transmission electron microscopy (TEM)

These experiments were performed with a Zeiss Libra 120 equipment located at the CITIUS. The samples were prepared by adding a drop of an aqueous solution of polymeric NPs ([NPs] = 1 mg/mL) on a cooper grid coated with a carbon film. Following this, it was air dried at room temperature. Subsequently, it was stained with uranyl acetate and dried before carrying out the measurements.

2.9. In vitro drug release

A solution of loaded NPs, of concentration close to 1.5 mg/mL, was suspended in a Tris/HCl buffer at pH=7.4 in a thermostated glass vial, at 37.4 °C, under continuous magnetic stirring (200 rpm). A sample was removed at determined time intervals, and afterwards centrifuged at 13500 rpm for 15 min, and replaced with an equal volume of the neutral buffer. This way the drug concentration in the release medium was diluted, mimicking the *in vivo* removal into the systemic circulation. After the centrifugation, the supernatant was taken and the amount of VRZ and CsA in the samples were determined by UV–visible spectroscopy and HPLC measurements, respectively. The experiments were repeated three times, and the experimental values are the average of the three replications.

Our aim was to test the formulated nanoparticles for treating *C. albicans* infections and avoiding biofilm formation since the antifungal activity of VRZ+CsA increased when both compounds were encapsulated together as compared to the free drugs. No administration route was considered because this research was beyond the scope of the present study. Nonetheless, the study of the release of the drugs at pH 7.4, the physiological pH, considered in the article provides interesting information for future work.

2.10. Antifungal susceptibility tests

Broth microdilution method performed according to the Clinical and Laboratory Standards Institute (CLSI) (Wayne, 2008) was followed to determine the Minimal Inhibitory Concentration (MIC) of the planktonic cells of the tested strain. In brief, stock solutions of free VRZ, CsA, and VRZ+CsA were prepared in DMSO at concentrations 100 times the highest concentration to be tested and then tenfold diluted in RPMI 1640

broth medium with L-glutamine and phenol red but without sodium bicarbonate (Sigma), buffered to pH 7.0 with 0.165 M MOPS (Sigma). Subsequently, the drug dilutions were further fivefold diluted with RPMI 1640, reducing the solvent concentration to 2 % DMSO and the compound to the two times strength needed in the test. Concurrently, NPs loaded with VRZ (NP-VRZ), CsA (NP-CsA), or VRZ+CsA (NP-VRZ+CsA), as well as unloaded NPs, were directly suspended in RPMI 1640 medium at 2X the concentration to be used for MIC determinations. To avoid NP aggregation, they were sonicated using an ultrasound probe (Digital Sonifier 450, Branson, USA) at 30 % amplitude during two cycles of 30 s, with a 30-seconds pause between them to prevent temperature rise. No filter-sterilization was required for stock solutions since they can be assumed to be sterile. The two times drug/NP concentrations were dispensed into the wells of the first column of a 96-microtiter plate and then twofold serially microdiluted throughout the columns. The yeast inoculum was prepared by randomly picking five colonies from 24-hour-old cultures of *C. albicans* grown on YPD agar at 35 °C. The colonies were suspended in 5 mL of sterile 0.9 % (w/v) saline solution and the turbidity adjusted to 0.13–0.14 at 530 nm wavelength. Afterward, the suspension was diluted 1:50 and then 1:20 with RPMI 1640 broth to obtain a working suspension containing *ca.* 10^3 planktonic cells/mL, which was further inoculated into each well of the microdilution tray. The final inoculum density achieved was 5×10^2 CFU/mL and the final concentrations of each antimicrobial compound ranged as follows: 256–0.0078 μg/ml for VRZ/NP-VRZ, 2048–16 μg/mL for CsA/NP-CsA, and 4/9.8–0.0312/0.077 μg/mL for VRZ+CsA/NP-VRZ+CsA. Blank unloaded NPs adjusted to the same concentration that the corresponding drug loaded NPs were also tested. Besides, growth controls (inoculation in wells without drugs/NPs) and sterile controls (wells without inoculum) were prepared. Microdilution plates were incubated at 35 °C and the detection of visible growth was read after 48 h. MICs were defined as the lowest drug concentration causing a 50 % decrease in turbidity as determined visually. All the experiments were performed in duplicate and repeated three times independently (biological triplicates).

2.11. Inhibition of biofilm formation

Biofilms of *C. albicans* formed in the presence of free and NP-encapsulated antifungal compounds were prepared following the same methodology and final drug concentrations as stated above for the susceptibility tests, with the exception that the final inoculum density in the microplate wells was adjusted to 8×10^4 CFU/mL to boost the biofilm development. Following incubation, the wells were washed twice with saline solution (0.9 %, w/v) to remove non-adhered planktonic cells. Next, an aliquot of 230 μL crystal violet 0.1 % (w/v) was added to each well to stain the biofilm. After 15 min at room temperature, the dye solution was removed, and the wells were rinsed three times with milliQ water. Then, 200 μL of 30 % (v/v) acetic acid was added to the wells to dissolve the stained biofilm and, finally, the mixture was aspirated, and the absorbance measured at $\lambda = 595$ nm using the Spark 20 M multimode Microplate Reader controlled by Spark Control™ software Version 2.1 (Tecan Group Ltd. Crailsheim, Germany).

2.12. Statistical analyses

Statistical analysis of anti-biofilm formation activity was carried out using one-way ANOVA followed by Dunnett's multiple-comparison test. Differences between free and encapsulated drugs were assessed for significance using the Student's *t*-test with a *P* value cutoff < 0.05. GraphPad Prism v10.2 software was employed to perform all the statistical tests.

For the release results, tests were done using the GraphPad Prism 8.0.1 software program (San Diego, CA). Statistics were determined with a two-way ANOVA Sidak' s multiple comparisons test.

3. Results and discussion

3.1. VRZ-loaded NPs

The encapsulation efficiency, %EE, and the synthesis yield, %R, for the different VRZ-loaded polymeric NPs are listed in Table 1. The results for the blank NPs are also showed in this table.

Table 1 shows that the synthesis yield is high and it is similar for the different prepared NPs. Besides, %R can be considered independent of the amount of VRZ used in the synthesis within experimental errors. In regard to the influence of the amount of VRZ on %EE, it can be observed that, initially, when the mg of voriconazole increases, no influence of the VRZ quantity used in the synthesis on this magnitude is observed. However, when this amount is larger than 10 mg a substantial decrease in %EE was found.

The zeta potential, ξ, size, and polydispersity index, PDI, of the unloaded and VRZ-loaded polymeric NPs are also listed in Table 1. Representative dynamic light scattering, DLS, histograms of VRZ-loaded NPs are shown in Figure S1 (Supplementary material).

The values summarized in Table 1 show that all the polymeric NPs have a negative zeta potential, in agreement with literature data for PLGA based NPs (López-López et al., 2019; Gossmann et al., 2015; Man et al., 2015; Arasoğlu and Derman, 2018; Ramzy et al., 2024; Folle et al., 2024). No dependence of the zeta potential on the amount of VRZ used in the synthesis is observed. The sizes of the prepared NPs from different PLGA derivates are not much different, although the PLGA+PEG NPs seem to be somewhat smaller than the PLGA and PLGA-PEG ones. The hydrodynamic diameter indicates that all the NPs prepared have a nano size. The PDI values do not depend on the initial amount of VRZ. As can be observed from the DLS histograms shown in Figure S1 (Supplementary material), PLGA and PLGA-PEG NPs present a unimodal size distribution, although for some amounts of VRZ, a bimodal distribution can be found (see Figure S1, Supplementary material). The PLGA+PEG NPs show a bimodal distribution for all the VRZ amounts, although the contribution of the first peak, corresponding to the smallest size of NPs, is low.

The morphology of the prepared NPs was examined by transmission electron microscopy, TEM. Fig. 2 shows the image for PLGA NPs (10 mg of VRZ). One can see that the NPs are spherical. The average size measured by TEM is around 350 nm, smaller than that obtained by DLS. This is an expected result since DLS measures the size of the NPs including the hydration layer, but TEM measurements are done on dried samples, as is described in the Experimental section. Anyway, the size found by using the two techniques agrees within experimental errors. Besides, no important polydispersity was observed in the TEM image, also in agreement with the DLS results.

The percentage of cumulative release *in vitro* for the VRZ-loaded PLGA, PLGA-PEG, and PLGA+PEG was studied (Figure S5, Supplementary material). As displayed in Figure S2 no initial burst was found for VRZ-loaded NPs, which points out that the drug is encapsulated within the NPs and not adsorbed at their surface. The release profiles correspond, in all cases investigated, to first order kinetic processes and they do not practically depend on the amount of drug used in the preparation method of the NPs. The release rate constants, k_r, were calculated by using Eq. (3):

$$\%\text{Cumulative release drug} = a\cdot(1 - \exp(-k_r\cdot t)) \quad (3)$$

where k_r is the first order rate constant corresponding to the drug release and *a* is and adjustable parameter. Solid lines in Figure S2 shows that the agreement between the experimental and the theoretical data is good. The rate constant values obtained were: $k_r=(8.4 \pm 0.4) \times 10^{-3}$ min^{-1} for PLGA, $k_r=(3.6 \pm 0.4) \times 10^{-2}$ min^{-1} for PLGA-PEG, and $k_r=(6.8 \pm 1.0)) \times 10^{-3}$ min^{-1} for PLGA+PEG. One can see that the release is faster in the case of PLGA-PEG, although the maximum amount of VRZ released from the different NPs follows the trend PLGA>PLGA-PEG>PLGA+PEG. Tests were done using the GraphPad

Table 1
Encapsulation efficiency, synthesis yield, hydrodynamic diameter, d_H, zeta potential, ξ, and polydispersity index, PDI, values obtained in the preparation of the unloaded and VRZ-loaded polymeric NPs at different amounts of VRZ (mg).

mg VRZ	Encapsulation efficiency, %EE	Synthesis yield, %R	Hydrodynamic diameter, d_H (nm)	Zeta potential, ξ (mV)	Polydispersity index, PDI
PLGA					
0	–	80 ± 4	453 ± 61	−18.5 ± 0.4	0.80 ± 0.07
5.0	20.1 ± 1.7	81 ± 3	388 ± 54	−19.2 ± 0.9	0.63 ± 0.07
7.5	17.9 ± 1.1	78 ± 3	442 ± 33	−24.6 ± 0.6	0.61 ± 0.10
10.0	18.8 ± 1.4	77 ± 2	387 ± 28	−24.9 ± 1.6	0.50 ± 0.02
15.6	19.4 ± 1.3	73 ± 3	486 ± 15	−20 ± 3	0.63 ± 0.10
PLGA-PEG					
0.0	–	84 ± 3	375 ± 36	−16.8 ± 0.4	0.72 ± 0.10
5.0	18.6 ± 1.3	86 ± 5	361 ± 68	−22.9 ± 1.1	0.50 ± 0.10
7.4	17.2 ± 1.1	88 ± 4	297 ± 65	−22.6 ± 1.1	0.45 ± 0.10
10.0	19.4 ± 1.4	85 ± 2	390 ± 44	−19.6 ± 0.4	0.50 ± 0.06
15.6	8.0 ± 0.9	84 ± 5	466 ± 78	−30 ± 2	0.6 ± 0.2
PLGA+PEG					
0.0	–	88 ± 6	372 ± 28	−18.9 ± 1.4	0.40 ± 0.04
5.0	25.0 ± 1.9	85 ± 4	334 ± 32	−32.6 ± 1.6	0.30 ± 0.10
7.5	18.8 ± 1.6	91 ± 6	309 ± 19	−34 ± 2	0.50 ± 0.08
10.2	21.1 ± 1.9	82 ± 3	411 ± 27	−32 ± 2	0.40 ± 0.07
16.0	9.0 ± 1.0	80 ± 5	364 ± 27	−30.0 ± 0.5	0.40 ± 0.07

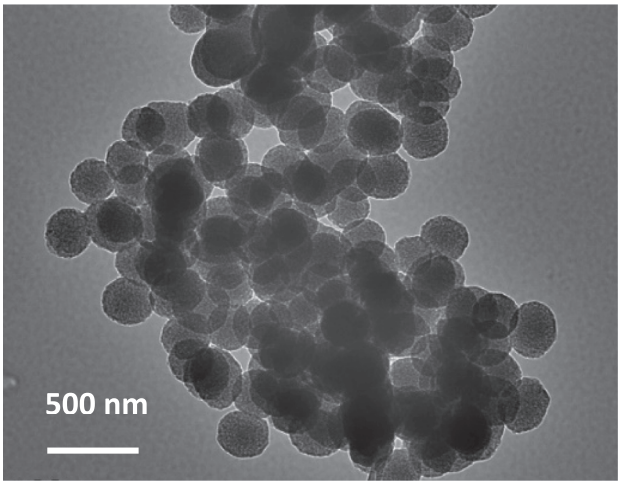

Fig. 2. TEM image of VRZ (10 mg) loaded-PLGA NPs.

Prism 8.0.1 software program (San Diego, CA). Statistics were determined with a two-way ANOVA Sidaks multiple comparisons test comparing the results obtained for the different types of polymeric NPs. Results shown in Figure S3 (Supplementary material) indicate that there is a significant difference between the release rate constants obtained in PLGA and PLGA+PEG and those estimated in PLGA-PEG, but no between those found in PLGA and PLGA+PEG.

3.2. CsA-loaded NPs

A similar characterization of the CsA-loaded NPs to that achieved for the VRZ-loaded NPs was carried out. Table 2 summarizes the data obtained. This Table shows that the encapsulation efficiency and the synthesis yield calculated for the CsA-loaded NPs do not depend on the amount of CsA initially used in the synthesis. All the NPs present a negative zeta potential, the values being within the same range as those found for VRZ loaded NPs. The sizes are also similar, considering experimental errors, and no dependence on the amount of CsA utilized was observed. Most of the CsA-loaded PLGA and PLGA-PEG NPs present a unimodal size distribution.

The representative DLS histograms shown in Figure S4 (Supplementary material) indicate that CsA-loaded NPs present a unimodal size distribution. The TEM image of CsA-loaded PLGA NPs (10 mg of CsA), shown in Fig. 3, present a spherical morphology and a size around 330 nm, in agreement with DLS results.

The percentage of cumulative release *in vitro* for the CsA-loaded PLGA, PLGA-PEG, and PLGA+PEG was studied (Figure S5, Supplementary material). As displayed in Figure S2 for VRZ, no initial burst was found for CsA-loaded NPs, which points out that, as in the case of VRZ, CsA is mainly encapsulated within the NPs. The release profiles correspond, in all cases investigated, to first order kinetic processes and they do not practically depend on the amount of drug used in the preparation method of the NPs. The release rate constants, k_r, were calculated by using eq. 3 (solid lines in Figure S5, Supplementary material), the results being $k_r=(9.3 \pm 0.4) \times 10^{-3}$ min^{-1} for PLGA, $k_r=(1.13 \pm 0.06) \times 10^{-2}$ min^{-1} for PLGA-PEG, and $k_r=(9.7 \pm 1.2)) \times 10^{-3}$ min^{-1} for PLGA+PEG. As in the case of VRZ, one can see that the release is faster in the case of PLGA-PEG, than in PLGA and PLGA+PEG. Similarly, the maximum amount of CsA released from the different NPs follows the trend PLGA>PLGA-PEG>PLGA+PEG. Tests were done using the same methodology as in the case of VRZ release. Results shown in Figure S6 (Supplementary material) indicate that there is a significant difference between the release rate constants obtained in PLGA and PLGA+PEG and those estimated in PLGA-PEG, but no between those found in PLGA and PLGA+PEG. Nonetheless, those differences are much smaller than in the case of VRZ (see Figures S3 and S6, Supplementary material).

3.3. (CsA+VRZ)-loaded PLGA NPs

The data listed in Tables 1 and 2 and the results retrieved from TEM and release experiments indicate that the best choice for carrying out the antifungal susceptibility and inhibition of biofilm formation tests are the loaded PLGA NPs with initial synthesis conditions of 10 mg of VRZ and 10 mg of CsA. These NPs were chosen because, although PLGA-PEG and PLGA+PEG also show good characteristics, the maximum amount of VRZ as well as of CsA released from these loaded NPs is smaller, around ½ and 1/3, than that observed for the PLGA NPs. Besides, PLGA+PEG NPs have a bimodal size distribution. The characterization of (VRZ+CsA)-loaded PLGA NPs (10 mg of VRZ+10 mg of CsA) is

Table 2
Encapsulation efficiency, synthesis yield, hydrodynamic diameter, d_H, zeta potential, ξ, and polydispersity index, PDI, values obtained in the preparation of the unloaded and CsA-loaded polymeric NPs at different amounts of CsA (mg).

mg CsA	Encapsulation efficiency, %EE	Synthesis yield, %R	Hydrodynamic diameter, d_H (nm)	Zeta potential, ξ (mV)	Polydispersity index, PDI
PLGA					
5.0	44 ± 4	80 ± 3	405 ± 62	−22.2 ± 1.6	0.51 ± 0.06
10.0	47 ± 3	77 ± 3	357 ± 26	−21.1 ± 1.1	0.42 ± 0.03
15.0	49 ± 5	75 ± 4	421 ± 15	−25 ± 2	0.60 ± 0.10
PLGA-PEG					
5.0	41 ± 3	78 ± 5	377 ± 76	−22.5 ± 1.1	0.52 ± 0.10
10.0	50 ± 4	80 ± 4	446 ± 39	−23 ± 1.3	0.40 ± 0.05
15.0	43 ± 4	80 ± 4	441 ± 72	−25 ± 2	0.61 ± 0.17
PLGA+PEG					
5.0	51 ± 5	82 ± 4	354 ± 29	−22.6 ± 1.6	0.40 ± 0.09
10.0	63 ± 4	81 ± 3	393 ± 24	−21.4 ± 1.5	0.60 ± 0.09
15.0	47 ± 5	81 ± 4	417 ± 42	−20.0 ± 0.9	0.47 ± 0.10

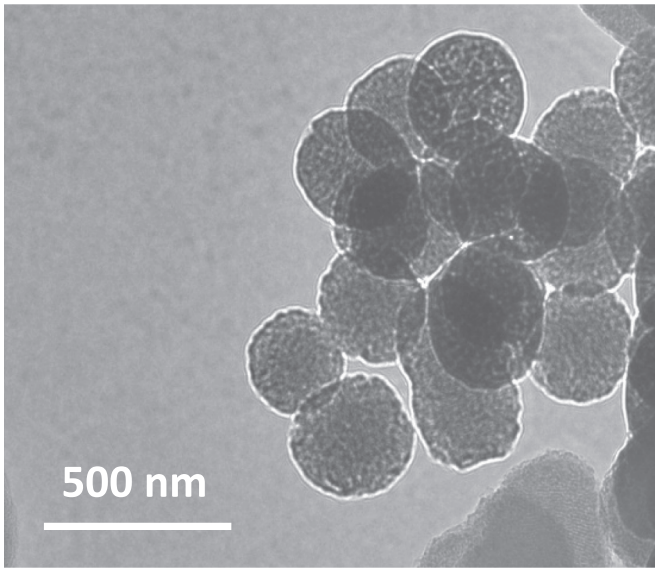

Fig. 3. TEM image of CsA (10 mg) loaded PLGA NPs.

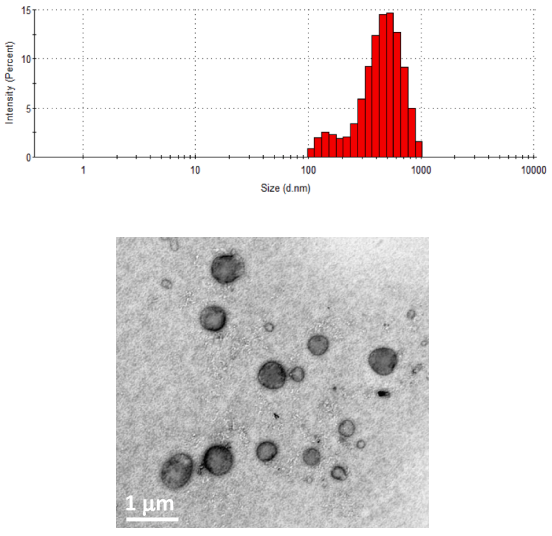

Fig. 4. Representative DLS histogram and TEM image corresponding to PLGA (10 mg VRZ+10 mg CsA)-loaded NPs.

presented below.

The estimated magnitudes corresponding to the VRZ+CsA (10 mg of VRZ+10 mg of CsA) loaded PLGA NPs were %EE VRZ=(18.2 ± 1.4)%, %EE CsA=(50 ± 4)%, %Y=(78 ± 4)%, ξ=(−26.0 ± 1.9) mV, d_H=561 ± 32 nm, and PDI=(0.49 ± 0.05).

A representative DLS histogram corresponding to the VRZ+CsA (10 mg of VRZ+10 mg of CsA)-loaded NPs investigated is shown in Fig. 4, together with their TEM image.

The VRZ and CsA encapsulation efficiencies observed when they are encapsulated together within the PLGA NPs are similar to those found for these NPs when the drugs are encapsulated separately. The synthesis yield and zeta potential are also such as those previously observed (Tables 1 and 2). However, the NPs are larger when the two drugs are encapsulated together compared to single drug loaded NPs. Besides, a bimodal size distribution was found. The TEM image shows NPs populations with different sizes, in agreement with the DLS observations. This issue will be considered again below:

The percentage of cumulative release *in vitro* of VRZ and CsA from the PLGA NPs (10 mg of VRZ+10 mg of CsA) was studied. Figure S7 (Supplementary material) shows the release profiles for the two drugs. One can see that the percentage of CsA releases is much higher than that of the VRZ, as was observed when the drugs were encapsulated separately in the different NPs studied (Figures S2 and S5, Supplementary material). The release data were fitted to a first order kinetic using eq. 3. The results were: $k_r=(6.7 \pm 0.2) \times 10^{-3}$ min^{-1} for VRZ, and $k_r=(8.4 \pm 0.5) \times 10^{-3}$ min^{-1} for CsA. Solid lines in Figure S7 (Supplementary material) show that there is an agreement between the experimental and the theoretical data. Tests were done as was commented above for VRZ and CsA releases. Results are shown in Figure S8 (Supplementary material). They indicate that there are significant differences between the release of both VRZ and CsA when they are alone or together into the PLGA NPs, being slower in the latter. The difference of the release rate between VRZ and CsA is significant and it is not much influenced by the fact that the two drugs are encapsulated separately or together.

At this point and considering again the issue of the bimodal size distribution, PLGA NPs encapsulating VRZ+CsA were prepared with different initial amounts of the two drugs. In particular, PLGA NPs (10 mg of VRZ+5 mg of CsA), PLGA NPs (7.5 mg of VRZ+5 mg of CsA), and PLGA NPs (7.5 mg of VRZ+10 mg CsA) were synthesized and their hydrodynamic diameter measured by DLS. In all cases the NPs were larger than those encapsulating the drugs separately and a bimodal size distribution was observed. Taking this into account, the biological

experiments were carried out with the PLGA NPs (10 mg of VRZ+10 mg of CsA).

3.4. Biological activity of drug loaded PLGA NPs against Candida albicans

Since previous studies have suggested the synergism between triazoles and the calcineurin inhibitor CsA (Shinde et al., 2012; Cordeiro et al., 2014; Nurrokhman Baly et al., 2015; Jia et al., 2016; Li et al., 2008; Zhang et al., 2019) and the enhancement of antifungal compounds following their encapsulation (Zhang et al., 2013; de Almeida Campos *et al.*, 2016; Kaur et al., 2021; Mohammadzadeh et al., 2021; Nami et al., 2021; Jangjou et al., 2022; Khare et al., 2016; Radwan et al., 2017; Badihi et al., 2020; Goyal et al., 2015; Duber *et al.*, 2015; li et al., 2023), here we decided to perform a preliminary exploration on the clinical potential of PLGA NPs loaded with VRZ and CsA, either independently encapsulated or as combined formulations. The susceptibility profile of the planktonic cells of the strain *C. albicans* ATCC 10231 showed the MIC ranges displayed in Table 3.

Considering the MIC breakpoints of the CLSI [39], the studied yeast was resistant to VRZ (as expected according to the strain description). Regarding CsA, the MIC values largely exceeded the general therapeutic range for this compound, which is not surprising given its clinical indication as immunosuppressant but not as antifungal drug. However, when both drugs are combined, they work synergistically and their MIC values drop dramatically, falling within the dosage window. Our MIC results agree with previous studies assessing the growth inhibition of *C. albicans* by triazoles and CsA, used separately or in combination (Li et al., 2008). Comparisons of MIC data between free and encapsulated drugs showed that, individually employed, VRZ and CsA have a slightly better, but not significant, effect (within a range of twofold concentration) if loaded into NPs. This MIC enhancement was also found for amphotericin B loaded PLGA-PEG NPs against *C. albicans* (Badihi et al., 2020). Nevertheless, the MIC for VRZ+CsA combination was reduced up to fourfold when the drugs were encapsulated in PLGA NPs. Considering that the blank unloaded NPs had no effect on the yeast growth at the maximum tested concentration, we can hypothesize that the improved activity of the encapsulated drugs may be due to the ameliorated drug stability, solubility, penetration, sustained release, and pharmacokinetics provided by the PLGA nanocarrier.

Biofilm development of *C. albicans* has been proved to be more susceptible to the synergistic effect of triazole compounds (including VRZ) combined with CsA than to triazole alone (Cordeiro et al., 2014; Nurrokhman Baly et al., 2015; Jia et al., 2016; Voltan et al., 2016). On the other hand, CsA alone exhibits a very poor or null ability to inhibit biofilm growth (Shinde et al., 2012; Cordeiro et al., 2014; Nurrokhman Baly et al., 2015; Jia et al., 2016; Nurrokhman Baly et al., 2015; Jia et al., 2016; Voltan et al., 2016). As in the previous findings (Nurrokhman Baly et al., 2015), our results also demonstrated that CsA concentrations ≥ 512 μg/mL were required to achieve an average biofilm reduction of 50 % or more (Fig. 5a). Free VRZ was able to prevent biofilm formation in more than a 50 % at all the tested concentrations (Fig. 5b), even though the planktonic cells of *C. albicans* ATCC 10231 were only susceptible at values ≥ 256 μg/mL (Table 3). However, the combined utilization of free VRZ+CsA allowed a twofold biofilm inhibition in comparison with the same concentration of free VRZ alone, in particular in the range 0.25–4 μg/mL of VRZ (Fig. 5 b,c). With regards to the encapsulated vs. the free drug effectiveness against biofilm formation, encapsulation results in an increase of the biological activity of the three tested treatments (CsA alone, VRZ alone, and VRZ+CsA) for most concentrations, although significant differences are observed only at moderate or low concentrations (Fig. 5). However, at high drug concentrations, inhibition of biofilm development was quite similar between free and encapsulated drugs (data not shown). At this point, it was necessary to consider if the biofilm reduction of drug loaded NPs could be due to the fungal activity of the PLGA nanoparticles themselves. Fig. 6 shows that blank PLGA NPs prevented the biofilm formation in more than a 50 % at high concentrations (≥0.179 mg/mL), but their antifungal effect was almost negligible or even biofilm promoting at lower concentrations (Fig. 6). This suggest that NPs do not have an additive effect over the drug, but they truly enhance its antifungal activity when used within the therapeutic window. That is, the

Table 3
In vitro antifungal activity against *C. albicans* ATCC 10231 of VRZ, CsA, and VRZ+CsA used as *free* and encapsulated drugs, as well as the biological activity of unloaded NPs.

Drug	MIC range (μg mL^{-1})		
	Free	loaded PLGA NPs (concentration of NPs)*	blank PLGA NPs
VRZ	256	128–256 (2864–5728)	>5728
CsA	512	256–512 (1580–3160)	>12640
VRZ+CsA	0.5–1/ 1.225–2.45	0.125–0.25/0.306–0.613 (5.547–11.094)	>177.5

*Concentration of NPs (μg mL^{-1}) in the microplate well to achieve the indicated drug concentration.

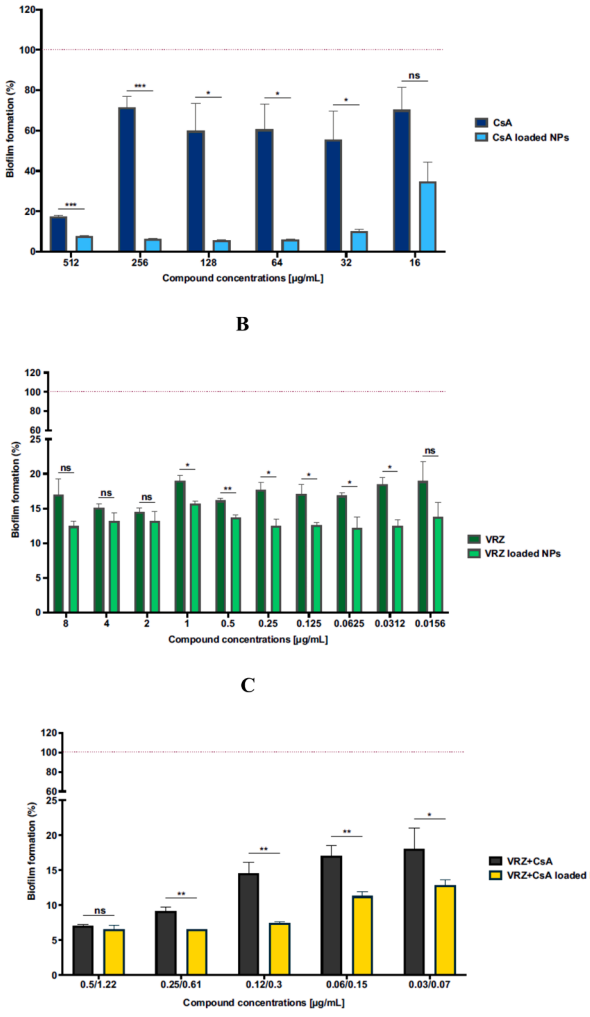

Fig. 5. Inhibition of biofilm formation exerted by **A)** CsA, **B)** VRZ, and **C)** VRZ+CsA treatments both as free and encapsulated formulations. The results are represented as the percentage of biofilm reduction in comparison with controls (red dotted line). The experiments were conducted in duplicate from three independent biological experiments (n = 6) and the data are expressed as mean ± SEM. ns, not significant (P>0.05); *, P<0.05; **, P<0.01; ***, P<0.001.

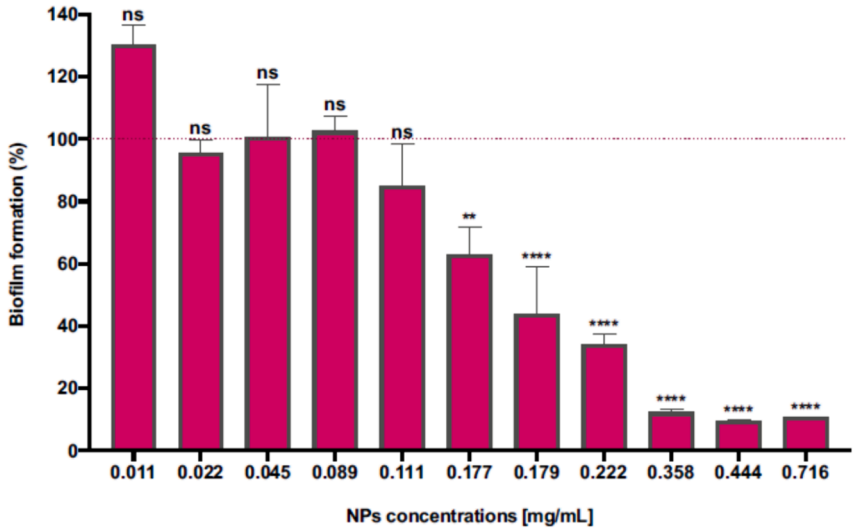

Fig. 6. Inhibition of biofilm formation exerted by the blank PLGA NPs. The results are represented as the percentage of biofilm reduction in comparison with controls (red dotted line). The experiments were conducted in duplicate from three independent biological experiments (n = 6) and the data are expressed as mean ± SEM. ns, not significant; **, $P<0.01$; ****, $P<0.0001$.

encapsulation of the drugs in polymeric NPs results in an increment of their fungal anti-biofilm effect.

4. Conclusions

Several PLGA based NPs were prepared with the goal of encapsulating VRZ and CsA, separately or together. The blank and loaded NPs were characterized and those with the most suitable properties were chosen to carry out the antifungal susceptibility tests and the inhibition of biofilm formation of *Candida albicans*. A synergistic effect between free VRZ and CsA was observed, the presence of CsA improving the antifungal activity of VRZ alone. When the drugs were encapsulated together in the NPs, an increment in the synergy was found, the antifungal activity of (VRZ+CsA)-loaded NPs increased fourfold as compared to that of free VRZ+CsA. With regard to the inhibition studies of *C. albicans* biofilm development, high concentrations of blank NPs suppressed the biofilm establishment. However, at low or moderate NPs concentrations, a negligible effect or even an increment in the biofilm formation was found. Therefore, the experimentally observed inhibition of the biofilm growth in the presence of encapsulated VRZ, CsA, or VRZ+CsA when compared with free drugs can be attributed to the encapsulation effects rather than to the polymeric NPs *per se*. Therefore, drug encapsulation, either separately or in combination, improved their antifungal activity against *C. albicans* biofilm development, when used within the therapeutic window.

As was commented above, various researchers have studied the synergistic effect between cyclosporine A and different antifungal agents such as voriconazole, fluconazole or caspofungin (Cordeiro et al., 2014; Jia et al., 2016; Zhang et al., 2019), when the drugs were free. The effect of voriconazole encapsulated in a variety of nanocarriers has also been investigated (de Almeida Campos et al., 2023; Das et al., 2015; Shah et al., 2022). However, to our knowledge, the synergistic behavior of VRZ and CsA when they are encapsulated together in nanovehicles has not been studied. The findings from the investigations done in this work lay a solid foundation for further exploration into the enhancement of the synergistic effect of other antifunfal agents, such as fluconazole, and CsA, when both are encapsulated together in nanocarriers, against the biofilm formation caused not only by *C. albicans*, but also by other strains such as *S. Candida glabrata, R. Candida krusei* or *C. metapsilosis*.

The goal of this manuscript was to test different nanoparticles formulations and assay their biological activity *in vitro*. The *ex vivo* and *in vivo* studies will certainly shed light on the clinical application of our drug loaded nanoparticles, but this is beyond the scope of the present research. Future research will address the detailed *ex vivo* and *in vivo* study of the antifugungal, antibiofilm, and toxicity analysis of the formulated nanoparticles. For this, collaborations with other research groups working with animal infection models will be required.

CRediT authorship contribution statement

Victoria Martín: Methodology, Investigation, Data curation. **Rafael R. de la Haba:** Writing – original draft, Resources, Methodology, Investigation. **Pilar López-Cornejo:** Writing – original draft, Supervision, Investigation, Funding acquisition, Conceptualization. **Manuel López-López:** Supervision, Investigation, Data curation. **José Antonio Lebrón:** . **Eva Bernal:** Supervision, Methodology, Investigation, Data curation. **Natalia Baeza:** Methodology, Investigation, Data curation. **Sara Ruiz:** Methodology, Investigation, Data curation. **Francisco José Ostos:** Supervision, Methodology, Data curation. **Vicente Merino-Bohorquez:** Resources, Investigation, Data curation. **Sylvie Chevalier:** Supervision, Resources, Methodology, Formal analysis, Data curation. **Olivier Lesouhaitier:** Supervision, Resources, Methodology, Formal analysis, Data curation. **Ali Tahrioui:** Resources, Methodology, Investigation, Formal analysis. **Francisco José Montes:** Methodology, Investigation, Data curation. **Teresa Sánchez-Carrasco:** Methodology, Investigation. **María Luisa Moyá:** Writing – original draft, Supervision, Investigation, Funding acquisition, Conceptualization.

Declaration of competing interest

The authors declare that they have no known competing financial interests or personal relationships that could have appeared to influence the work reported in this paper.

Data availability

Data will be made available on request.

Acknowledgements

This work was financied by the Consejería de Economía, Conocimiento, Empresas y Universidades de la Junta de Andalucía (FQM-206, FQM-274), the European Union (Feder Funds), and by the University of Seville (Ayudas Servicios Generales de la Universidad, CITIUS,

2024/00000387, 2024/00000395). The authors acknowledge the postdoctoral grant of F.J. Ostos (PAIDI-DOCTOR, Junta de Andalucía with European Social Fund, DOC_00963).

Appendix A. Supplementary data

Supplementary data to this article can be found online at https://doi.org/10.1016/j.ijpharm.2024.124593.

References

Akbari, F., Kjellerup, B.V., 2015. Elimination of bloodstream infections associated with *Candida albicans* biofilm in intravascular catheters. Pathogens 4, 457–469. https://doi.org/10.3390/pathogens4030457.

Arasoğlu, T., Derman, S., 2018. Assessment of the antigenotoxic activity of poly(D, L–lactic-co-glycolic acid) nanoparticles loaded with caffeic acid phenethyl ester using the Ames *Salmonella*/microsome assay. J. Agric. Food Chem. 66, 6196–6204. https://doi.org/10.1021/acs.jafc.8b01622.

Badihi, A., Frušić-Zlotkin, M., Soroka, Y., Benhamron, S., Tzur, T., Nassau, T., Benita, S., 2020. Topical nano-encapsulated cyclosporine formulation for atopic dermatitis treatment. Nanomedicine 24, 102140. https://doi.org/10.1016/j.nano.2019.102140.

Cheng, L., Xiang, R., Liu, L., Li, Y., Chen, H., Yao, P., Sun, F., Xia, P., 2020. Therapeutic drug monitoring and safety of voriconazole in elderly patients. Int. Immunopharmacol. 78, 106078 https://doi.org/10.1016/j.intimp.2019.106078.

Cordeiro, R.A., Macedo, R.B., Teixeira, C.E.C., Marques, F.J.F., Bandeira, T.J.P.G., Moreira, J.L.B., Samia, R., Brilhantre, N., Rocha, G., Costa Sidrim, J.J., 2014. The calcineurin inhibitor cyclosporin A exhibits synergism with antifungals against *Candida parapsilosis* species complex. J. Med. Microbiol. 63, 936–944. https://doi.org/10.1099/jmm.0.073478-0.

Das, P.J., Paul, P., Mukherjee, B., Mazumder, B., Modal, L., Baisshya, R., Debnath, M.C., Dey, K.S., 2015. Pulmonary delivery of voriconazole loaded nanoparticles providing a prolonged drug level in lungs: A promise for treating fungal infection. Mol. Pharmaceutics 12, 2651–2664. https://doi.org/10.1021/acs.molpharmaceut.5b00064.

David, F., Rodrigues Morais, J., Beires, F., Greefield, H., Fernandes, G.L., 2022. Invasive pulmonary Aspergillosis after COVID-19 pneumonia. eCollection 2022 Eur. J. Case Rep. Intern. Med. 9, 003209. https://doi.org/10.12890/2022_003209.

de Almeida Campos, L., Fin, M.T., Santos, K.S., de Lima Gualque, M.W., Freire Cabral, A. K.L., Khalil, N.M., Fusco-Almeida, A.M., Mainardes, R.M., Soares Giannina, M.J., 2023. Nanotechnology-based approaches for voriconazole delivery applied to invasive fungal infections. Pharmaceutics 15, 266. https://doi.org/10.3390/pharmaceutics15010266.

Deleuran, M., Dezfoulian, B., Elberling, J., Knutar, I., Lapeere, H., Lossius, A.H., Schuttelaar, M.L.A., Stockman, A., Wikstrom, E., Bradley, M., de Bruin-Weller, M., Gutermuth, J., Mandelin, J.M., Schmidt, M.C., Thyssen, J.P., Vestergaard, C., 2024. Systemic anti-inflammatory treatment of atopic dermatitis during conception, pregnancy and breastfeeding: Interdisciplinary expert consensus in Northern Europe. J. Eur. Acad. Dermatol. Venereol. 38, 31–41. https://doi.org/10.1111/jdv.19512.

Donnelly, J.P., de Pauw, B.E., 2004. Voriconazole–a new therapeutic agent with an extended spectrum of antifungal activity. Clin. Microbiol. Infect. 10, 107–117. https://doi.org/10.1111/j.1470-9465.2004.00838.x.

Duber, P., Barker, S.A., Craig, D.Q.M., 2020. Design and characterization of cyclosporine a-loaded nanofibers for enhanced drug dissolution. ACS Omega 5, 1003–1013. https://doi.org/10.1021/acsomega.9b02616.

Folle, C., Marques, A.M., Mallandrich, M., Suñer-Carbó, J., Halbaut, L., Sánchez-López, E., López-Machado, A.L., Díaz-Garrido, N., Badía, J., Balldoma, L., Espina, M., García, M.L., Calpena, A.C., 2024. Colloidal hydrogel systems of thymol-loaded PLGA nanoparticles designed for acne treatment. Colloids Surf. B Biointerfaces 234, 113678. https://doi.org/10.1016/j.colsurfb.2023.113678.

Gossmann, R., Fahrländer, E., Hummel, M., Mulac, D., Brockmeyer, J., Langer, M., 2015. Comparative examination of adsorption of serum proteins on HSA- and PLGA-based nanoparticles using SDS-PAGE and LC-MS. Eur. J. Pharm. Biopharm. 93, 80–87. https://doi.org/10.1016/j.ejpb.2015.03.021.

Goyal, R., Macri, L., Kohn, J., 2015. Delivery of cyclosporine A: comparison of two polymeric nanospheres. Sci. Rep. 5, 13065. https://doi.org/10.1038/srep13065.

Guareschi, F., del Favero, E., Ricci, C., Cantu, L., Brandolini, M., Sambri, V., Nicoli, S., Pescina, S., ÍAngelo, D., Rossi, I., Buttini, F., Bettini, R., Sonvico, F., 2024. Cyclosporine A micellar nasal spray characterization and antiviral action against SARS-CoV-2. European J. Pharm. Sci. 193, 106673. https://doi.org/10.1016/j.ejps.2023.106673.

Gushiken, A.C., Saharia, K.K., Baddley, J.W., 2021. *Cryptococcus neoformans* Csn1201 is associated with pulmonary immune responses and disseminated infection? Infect. Dis. Clin. N. Am. 35, 493–514. https://10.3389/fimmu.2022.890258.

Jangjou, A., Zareshahrabadi, Z., Abbasi, M., Kamyab, H., Chelliapan, S., Baez, A., Golchin, A., Tayebi, L., Vara, E., Amani, A.M., Faramarzi, H., 2022. Time to conquer fungal infectious diseases: employing nanoparticles as powerful and versatile antifungal nanosystems against a wide variety of fungal species. Sustainability 14, 12942.

Jia, W., Zhang, H., Li, C., Li, G., Liu, X., Wei, J., 2016. The calcineruin inhibitor cyclosporine a synergistically enhances the susceptibility of *Candida albicans* biofilms to fluconazole by multiple mechanisms. BMC Microbiol. 16, 113. https://doi.org/10.1186/s12866-016-0728-1.

Johnson, L.B., Kauffman, C.A., 2003. Voriconazole: a new triazole antifungal agent. Clin. Infect. Dis. 36, 630–637. https://doi.org/10.1086/367933.

Kaur, R., Dennison, S.R., Burrow, A.J., Rudramurthy, S.M., Swami, R., Gorki, V., Katare, O.P., Kaushik, A., Singh, B., Singh, K.K., 2021. Nebulised surface-active hybrid nanoparticles of voriconazole for pulmonary *Aspergillosis* demonstrate clathrin-mediated cellular uptake, improved antifungal efficacy and lung retention. J. Nanobiotechnology 19, 19. https://doi.org/10.1186/s12951-020-00731-1.

Khare, A., Singh, I., Pawar, P., Grover, K., 2016. Design and evaluation of voriconazole loaded solid lipid nanoparticles for ophthalmic application. J. Drug Deliv. 2016, 6590361. https://doi.org/10.1155/2016/6590361.

Li, Y., Sun, S., Guo, Q., Ma, L., Shi, C., Su, L., Li, H., 2008. *In vitro* interaction between azoles and cyclosporin A against clinical isolates of *Candida albicans* determined by the chequerboard method and time-kill curves. J. Antimicrob. Chemother. 61, 577–585. https://doi.org/10.1093/jac/dkm493.

Li, S., Wu, T., Wu, J., Zhou, J., Yang, H., Chen, L., Zhang, D., 2023. Cyclosporine A-Encapsulated pH/ROS dual-responsive nanoformulations for the targeted treatment of colitis in mice. ACS Biomater. Sci. Eng. 9, 5737–5746. https://doi.org/10.1021/acsbiomaterials.3c01191.

Locatelli, E.V.T., Acuna, K.A., Betz, J., Tovar, A.A., Galor, A., 2024. Comparison of subjective responses to cyclosporine 0.05% versus lifitegrast 5.0% in individuals with dry eye disease. Cornea 43, 88–94. https://doi.org/10.1097/ICO.0000000000003266.

López-López, M., Fernández-Delgado, A., Moyá, M.L., Blanco-Arévalo, D., de la Carrera, C., Haba, R.R., Ventosa, A., López-Cornejo, P., 2019. Optimized preparation of levofloxacin loaded polymeric nanoparticles. Pharmaceutics 11, 57. https://doi.org/10.3390/pharmaceutics11020057.

Man, D.K.W., Casettari, L., Cespi, M., Bonacucina, G., Palmieri, G.F., Sze, S.C.W., Leung, G.P.H., Lam, J.K.W., Kwok, P.C.L., 2015. Oleanolic acid loaded PEGylated PLA and PLGA nanoparticles with enhanced cytotoxic activity against cancer cells. Mol. Pharm. 12, 2112–2125. https://doi.org/10.1021/acs.molpharmaceut.5b00085.

Mohammadzadeh, S., Shahsavari, S., Karimian, F., Hashemi, S.J., Javan, H.A., Mollabagher, H., 2021. Development and characterization of optimized sustained release voriconazole-loaded chitosan nanoparticles for ocular delivery. Particle. Sci. Tecnol. 7, 1–10. https://doi.org/10.22104/jpst.2021.4769.1183.

Nami, S., Aghebati-Maleki, A., Aghebati-Maleki, L., 2021. Current applications and prospects of nanoparticles for antifungal drug delivery. EXCLI J. 20, 562–584. https://doi.org/10.17179/excli2020-3068.

Nurrokhman Baly, I., Daeli, P.R., Kartasasmita, G., Wijayanti, N., 2015. Cyclosporine A decreases the fluconazole minimum inhibitory concentration of *Candida albicans* clinical isolates but not biofilm formation and cell growth. Trop. Biomed. 32, 176–182. https://doi.org/10.1186/s12866-016-0728-1.

Otto, W.R., Green, A.M., 2020. Fungal infections in children with haematologic malignancies and stem cell transplant recipients. Br. J. Haematol. 189, 607–624. https://doi.org/10.1111/bjh.16452.

Pinto Reis, C., Neufeld, R.J., Ribeiro, A.J., Veiga, F., 2006. Nanoencapsulation I. Methods for preparation of drug-loaded polymeric nanoparticles. Nanomedicine 2, 8–21. https://doi.org/10.1016/j.nano.2005.12.003.

Radwan, M.A., AlQuadeib, B.Y., Šiller, L., Wright, M.C., Horrocks, B., 2017. Oral administration of amphotericin B nanoparticles: antifungal activity, bioavailability and toxicity in rats. Drug Deliv. 24, 40–50. https://doi.org/10.1080/10717544.2016.1228715.

Ramzy, A., Soliman, A.H., Hassanein, S.I., Sebak, A.A., 2024. Multitarget, multiagent PLGA nanoparticles for simultaneous tumor eradication and TME remodeling in a melanoma mouse model. Drug Deliv. Transl. Res. 14, 491–509. https://doi.org/10.1007/s13346-023-01413-9.

Rosa, A.C., Finocchietti, M., Agabit, N., Mene, P., Bracaccia, M.E., Bellini, A., Massari, A. M., Alegiani, S.S., Masiero, L., Bedeschi, G., Cardillo, M., Lecenteforte, E., Piccolo, G., Leoni, O., Ferroni, E., Pierobon, S., Nordio, M., Ledda, S., Garau, D., Davoli, M., Addis, A., Belleudi, V., 2023. Determinants of immunosuppressive therapy in renal transplant recipients: an Italian observational study (the CESIT project). BMC Nephrol. 24, 320. https://doi.org/10.1186/s12882-023-03325-9.

Shah, M.K.A., Azad, A.K., Nawaz, A., Ullah, S., Latif, M.S., Rahman, H., Alsharif, K.F., Alzahrani, K.J., El-Kott, A.F., Albrakati, A., Abdel-Daim, M.M., 2022. Formulation development, characterization, and antifungal evaluation of chitosan NPs for topical delivery of voriconazole *in vitro* and *ex vivo*. Polymers 14, 135. https://doi.org/10.3390/polym14010135.

Shi, C., Xiao, Y., Mao, Y., Wu, J., Lin, N., 2019. Voriconazole: a review of population pharmacokinetic analyses. Clin. Pharmacokinet. 58, 687–703. https://doi.org/10.1007/s40262-019-00735-7.

Shinde, R.B., Chauhan, N.M., Raut, J.S., Karuppayil, S.M., 2012. Sensitization of *Candida albicans* biofilms to various antifungal drugs by cyclosporine A. Ann. Clin. Microbiol. Antimicrob. 11, 27. https://doi.org/10.1186/1476-0711-11-27.

Taff, H.T., Nett, J.E., Zarnowski, R., Ross, K.M., Sanchez, H., Cain, M.T., Hamaker, J., Mitchell, A.P., Andes, D.R., 2012. *Candida* biofilm-induced pathway for matrix glucan delivery: implications for drug resistance. PLoS Pathog. 8, e1002848.

Theuretzbacher, U., Ihle, F., Derendorf, H., 2006. Pharmacokinetic/pharmacodynamic profile of voriconazole. Clin. Pharmacokinet. 45, 649–663.

Uppuluri, P., Nett, J., Heitman, J., Andes, D., 2008. Synergistic effect of calcineurin inhibitors and fluconazole against *Candida albicans* biofilms. Antimicrob. Agents Chemother. 52, 1127–1132. https://doi.org/10.1128/AAC.01397-07.

Vila, T., Sultan, A.S., Montelongo-Jauregui, D., Jabra-Rizk, M.A., 2020. Oral Candidiasis: a disease of opportunity. J. Fungi 6. https://doi.org/10.3390/jof6010015.

Voltan, A.R., Quindós, G., Alarcón, K.P.M., Fusco-Almeida, A.M., Mendes-Giannini, M.J. S., Chorilli, S., 2016. Fungal diseases: could nanostructured drug delivery systems be a novel paradigm for therapy? Int. J. Nanomedicine 11, 3715–3730. https://doi.org/10.2147/IJN.S93105.

Wayne, P.A., 2008. Clinical and Laboratory Standards Institute. Reference method for broth dilution antifungal susceptibility testing of yeasts; approved standard–Third Edition M27–A3. Clinical and Laboratory Standards Institute.

WHO. Fungal priority pathogens list to guide research, development and public health action. World Health Organization: Geneva, Switzerland, 2022.

Wu, S., Wang, Y., Liu, N., Dong, N., Sheng, C., 2017. Tackling fungal resistance by biofilm inhibitors. J. Med. Chem. 60 (2017), 2193–2211. https://doi.org/10.1021/acs.jmedchem.6b01203.

Zhang, L., Keogh, S., Rickard, C.M., 2013. Reducing the risk of infection associated with vascular access devices through nanotechnology: a perspective. Int. J. Nanomedicine 8, 4453–4466. https://doi.org/ 10.2147/IJN.S50312.

Zhang, M., Yang, X., Wang, D., Yu, C., Sun, S., 2019. Antifungal activity of immunosuppressants used alone or in combination with fluconazole. J. Appl. Microbiol. 126, 1304–1317. https://doi.org/10.1111/jam.14126.